Energy Conversion and Management 93 (2015) 215–227

Contents lists available at ScienceDirect

Energy Conversion and Management

journal homepage: www.elsevier.com/locate/enconman

Diurnal thermal analysis of microencapsulated PCM-concrete composite walls

Alexander M. Thiele [a], Gaurav Sant [b,c], Laurent Pilon [a,*]

[a] Mechanical and Aerospace Engineering Department, University of California, Los Angeles, Henry Samueli School of Engineering and Applied Science, United States
[b] Civil and Environmental Engineering Department, Laboratory for the Chemistry of Construction Materials (LC^2), University of California, Los Angeles, Henry Samueli School of Engineering and Applied Science, United States
[c] California Nanosystems Institute (CNSI), University of California, Los Angeles, Henry Samueli School of Engineering and Applied Science, United States

ARTICLE INFO

Article history:
Received 27 August 2014
Accepted 25 December 2014

Keywords:
Phase change materials
Microencapsulated
Building materials
Energy efficient building
Effective thermal properties

ABSTRACT

This paper examines the benefits of adding microencapsulated phase change material (PCM) to concrete used in building envelopes to reduce energy consumption and costs. First, it establishes that the time-dependent thermal behavior of microencapsulated PCM-concrete composite walls can be accurately predicted by an equivalent homogeneous wall with appropriate effective thermal properties. The results demonstrate that adding microencapsulated PCM to concrete resulted in a reduction and a time-shift in the maximum heat flux through the composite wall subjected to diurnal sinusoidal outdoor temperature and solar radiation heat flux. The effects of the PCM volume fraction, latent heat of fusion, phase change temperature and temperature window, and outdoor temperature were evaluated. Several design rules were established including (i) increasing the PCM volume fraction and/or enthalpy of phase change increased the energy flux reduction and the time delay, (ii) the energy flux reduction was maximized when the PCM phase change temperature was close to the desired indoor temperature, (iii) the optimum phase change temperature to maximize the time delay increased with increasing average outdoor temperature, (iv) in extremely hot or cold climates, the thermal load could be delayed even though the reduction in daily energy flux was small, and (v) the choice of phase change temperature window had little effect on the energy flux reduction and on the time delay. This analysis can serve as a framework to design PCM composite walls in various climates and seasons and to take advantage of time of use electricity pricing.

1. Introduction

In 2011 in the United States, residential and commercial building operation represented about 40% of the total end-use energy consumed [1]. About 40% of this energy was consumed for heating, ventilation, and air conditioning (HVAC) [2]. The demand of residential and commercial buildings for electricity varies significantly during the day [3]. To satisfy demand during peak hours, the utilities rely on so-called "*peaker plants*," which are costly to operate and typically run on fossil fuel [4]. In addition, utility companies offer time of use (TOU) electricity rate schedules to encourage ratepayers to shift their electricity use to off-peak hours. In practice, the price of electricity is lower during off-peak hours and higher during peak hours. To curb the energy consumption of the building sector, the 2008 California long term energy efficiency strategic plan established two major goals: (1) all new residential buildings should be zero net energy (ZNE) by 2020 and (2) all new commercial buildings by 2030 [5].

Building energy consumption could be reduced by using dynamic building envelope materials that control the heat flow into and out of buildings. Composite cementitious materials containing microencapsulated phase change materials (PCMs) have been suggested as a way to increase buildings' thermal inertia and thus their energy efficiency [6–8]. PCMs store energy in the form of latent heat by reversibly changing phase between solid and liquid. The goal in implementing composite PCM walls is to significantly reduce and time-shift the maximum thermal load on the building in order to reduce and smooth out the electricity demand for heating and cooling. This could also help ratepayers take advantage of TOU electricity rate schedules while reducing the ecological footprint of buildings [3,4,9–12]. The choice of PCM should be adapted to the climate and building orientation so as to maximize the above mentioned benefits.

* Corresponding author. Tel.: +1 (310) 206 5598; fax: +1 (310) 206 2302.
E-mail address: pilon@seas.ucla.edu (L. Pilon).

http://dx.doi.org/10.1016/j.enconman.2014.12.078
0196-8904/

Nomenclature

a	length of cubic unit cell, μm
A_c	cross-sectional area, m^2
$c_{p,j}$	specific heat of phase "j" in the composite structure, J/kg K
D	diameter, μm
E_r	energy flux reduction, %
h_i, h_o	indoor and outdoor convective heat transfer coefficient, W/m^2 K
h_{sf}	latent heat of fusion, J/kg
H	enthalpy, J
k_j	thermal conductivity of phase "j" in the composite structure, W/m K
L	wall thickness, mm or cm
$\mathbf{n}$	normal unit vector
Q''	energy flux, J/m^2
q''_s	solar radiation heat flux, W/m^2
q''_x, q''_y, q''_z	heat flux along the x-, y-, and z-directions, W/m^2
$\mathbf{r}$	position vector $\mathbf{r} = \langle x, y, z \rangle$
t	time, s
t_{max}	time of maximum heat flux through composite wall, h
$t_{max,m}$	time of maximum heat flux through pure concrete wall, h
T	temperature, °C
$T_{in}, T_\infty, T_{sky}$	indoor, ambient, and sky temperatures, °C
T_{max}, T_{min}	maximum and minimum outdoor temperatures, °C
V	volume, m^3

Greek symbols

α	thermal diffusivity, m^2/s
α_s	surface solar absorptivity
ΔT_{pc}	phase change temperature window, °C
Δx	minimum mesh size, μm
ϵ	surface emissivity
$\phi_{c/s}$	volume fraction of core with respect to shell material in a microcapsule
ϕ_j	volume fraction of phase "j" in the composite structure
ρ_j	density of phase "j" in the composite structure, kg/m^3
σ	Stefan–Boltzmann constant, W/m^2 K^4
τ_d	time delay, i.e. $\tau_d = t_{max} - t_{max,m}$, h

Subscripts

c	refers to core material (PCM)
eff	refers to effective properties
i	refers to initial conditions
j	refers to constituent material "j"
l	refers to PCM liquid phase
L	refers to values at $x = L$
m	refers to matrix (concrete)
max	refers to maximum value of variable
min	refers to minimum value of variable
opt	refers to optimum values
s	refers to PCM solid phase or shell
t	refers to total quantities

This study aims to evaluate the effects of adding microencapsulated PCMs to a concrete wall on buildings' thermal load. First, simulation tools and effective medium approximations (EMAs) were implemented to simulate, simply and accurately, transient heat transfer through three-component composite walls consisting of core–shell microcapsules embedded in a continuous matrix. Then, a parametric study was performed to determine the effects of the PCM properties on the reduction and delay of thermal load through such composite walls subjected to diurnal sinusoidal outdoor temperature and solar radiation heat flux. This study will serve as a framework for the design of composite walls containing microencapsulated PCM for energy efficient buildings in various climates.

2. Background

2.1. Building materials containing PCM

The use of composite building materials containing PCMs has been reviewed extensively [8,13–20] and need not be repeated. The forms of PCM composite walls that have received the most attention include wallboard (i.e., plasterboard or drywall), shape stabilized PCM (SSPCM) board, and PCM-concrete composites, as well as masonry blocks and alternative containers made of PVC or aluminum foil [14,18,20]. Methods of adding PCMs into building materials generally fall into four categories: (i) direct incorporation, (ii) immersion, (iii) macroencapsulation, and (iv) microencapsulation [20]. Direct incorporation consists of adding PCMs to supporting materials, such as wallboard or concrete, during the production process. Immersion method involves dipping a finished porous building material into melted PCM. Major drawbacks of these two methods include the lack of a barrier to protect the PCM against leakage during melting and against chemical reactions with the matrix material [18,19]. To address this issue, macroencapsulation of PCMs in containers such as bags, tubes, or panels has been proposed before incorporating the encapsulated PCM into composite walls [13,20]. However, macroencapsulation suffers from a large temperature differential between the encapsulated PCM core and the boundary which can lead to incomplete melting or solidification of the PCM [13,20,21]. This can be addressed by containing PCMs in microscopic capsules with thin walls and diameter ranging from 1 μm to 1 mm [21,22]. The microencapsulated PCM can easily be added to a building material during production as long as the shell material is compatible with the supporting material [13,20,21].

Concrete is an appealing construction material thanks to its inherently large thermal inertia. In fact, concrete has a significantly larger volumetric heat capacity than gypsum wallboard due to its higher density [8]. It has been suggested that PCM could be encapsulated prior to incorporation into concrete to prevent leakage and to ensure that it does not react with the concrete constituents [8,23]. Hunger et al. [23] studied the effect of adding microencapsulated PCM to self-compacting concrete on the effective thermal and mechanical properties of the composite. They found that the compressive strength of their specific mixture decreased by 13% for every additional mass percentage of PCM. The effective thermal conductivity of the composite also decreased with the addition of PCM. They concluded that composite concrete with a PCM content of 3 wt.% and a compressive strength of 35 N/mm^2 was acceptable for most building applications. Cabeza et al. [6] constructed cubicles made with plain concrete and with concrete containing 5 wt.% microencapsulated PCM. The cubicles were exposed to weather conditions in Lleida, Spain and temperatures were measured at the inner wall surfaces. The PCM concrete cubicle featured a 3 °C decrease in the amplitude of indoor temperature oscillations and a 2 h shift in the maximum indoor temperature compared with its counterpart made of plain concrete.

2.2. Simulating phase change in single phase systems

Analytical solutions of solid–liquid phase change heat transfer problems are only available for homogeneous systems with simple

geometries and boundary conditions [7,24,25]. As a result, numerical methods have been devised to model heat transfer during solid–liquid phase change including (i) the enthalpy method, (ii) the heat capacity method, (iii) the temperature transforming model, and (iv) the heat source method [24]. The advantages, disadvantages, and limitations of each method have been reviewed by Al-Saadi and Zhai [24]. The enthalpy method [25–29] and heat capacity method [26,27,30,31] are the two most commonly used numerical methods [7].

The enthalpy method consists of solving the transient heat conduction equation expressed in terms of temperature and enthalpy $H(T)$ as [26],

$$\frac{\partial \rho H(T)}{\partial t} = \nabla(k \nabla T) \tag{1}$$

where ρ and k are the density and thermal conductivity of the PCM, respectively. The enthalpy function $H(T)$ represents the total energy of the material including sensible and latent forms of energy. The enthalpy of a PCM can be determined as a continuous function of temperature by using differential scanning calorimetry (DSC) measurements [32]. Otherwise, a piecewise enthalpy function $H(T)$ may be defined in terms of the latent heat of fusion h_{sf} and the phase change temperature window ΔT_{pc} [25,28,29].

Alternatively, the heat capacity method consists of solving the transient heat conduction equation expressed in terms of temperature and specific heat $c_p(T)$ as [26,30,27,31],

$$\rho c_p(T) \frac{\partial T}{\partial t} = \nabla(k \nabla T) \tag{2}$$

To account for the latent heat stored during phase transition, the specific heat is defined as a piecewise function of temperature given by Lamberg et al. [27],

$$c_{p,c}(T) = \begin{cases} c_{p,c,s} & \text{for} \quad T < T_{pc} - \Delta T_{pc}/2 \\ c_{p,c,s} + \frac{h_{sf}}{\Delta T_{pc}} & \text{for} \quad T_{pc} - \Delta T_{pc}/2 \leqslant T \leqslant T_{pc} + \Delta T_{pc}/2 \\ c_{p,c,l} & \text{for} \quad T > T_{pc} + \Delta T_{pc}/2 \end{cases} \tag{3}$$

where $c_{p,c,s}$ and $c_{p,c,l}$ are the specific heats of the solid and liquid phase, respectively. Here, h_{sf}, T_{pc}, and ΔT_{pc} are the latent heat of fusion, the phase change temperature, and the temperature windows, respectively.

Lamberg et al. [27] experimentally studied heat transfer through a homogeneous paraffin PCM block contained in a rectangular aluminum enclosure. The PCM temperature was measured using thermocouples placed at various locations in the enclosure. The authors compared the measured local temperatures to numerical predictions obtained by implementing both the enthalpy and the heat capacity methods. They concluded that both numerical methods provided a "*good estimation*" of melting and freezing processes but that the heat capacity method agreed more closely with experimental data.

2.3. Simulating phase change in PCM composites

Zhou et al. [33] numerically simulated a room in a skyrise with one south-facing exterior wall and three interior walls. The multilayer ceiling and walls had either a mixed PCM-gypsum or a shape-stabilized PCM (SSPCM) composite layer at the inner surface. Time-dependent outdoor temperature and solar radiation heat flux were imposed on the exterior wall to reflect a typical winter week in Beijing, China. The authors modeled phase change using the enthalpy method and studied the effect of phase change temperature T_{pc} and temperature window ΔT_{pc} on the indoor temperature. The amplitude of the temperature oscillations was found to decrease with decreasing phase change temperature window ΔT_{pc}. It could be reduced by as much as 46% and 56% for mixed PCM-gypsum and SSPCM layers, respectively, compared with a plain gypsum board layer. They also found that the optimal phase change temperature T_{pc} to minimize the amplitude of the indoor temperature oscillations was 21 °C for both mixed PCM-gypsum and for SSPCM layers. In another study, Zhou et al. [34] simulated the same room with multilayer ceiling and walls containing a SSPCM composite layer on a different winter week in Beijing, China. Once again, the amplitude of temperature oscillations was minimized for a phase change temperature T_{pc} of 20 °C, which was within the range of indoor comfort temperature.

Diaconu and Cruceru [35] conducted a numerical study of a room with multilayer exterior walls consisting of an insulation layer between two PCM wallboards. Time-dependent temperature and solar radiation heat flux were imposed at the outer surface of the walls to reflect yearly averaged annual weather conditions in Bechar, Algeria. Each PCM-wallboard layer was assumed to be homogeneous with some arbitrarily chosen effective thermal properties. The enthalpy method was used to simulate phase change. The cooling/heating load on the room was determined by performing an energy balance on the indoor space. The authors evaluated the effects of phase change temperature T_{pc} and temperature window ΔT_{pc} in each PCM wallboard on the total annual heating and cooling energy reduction and on the reduction of the peak heating and cooling loads. Unlike Zhou et al. [33], they found that ΔT_{pc} had very little effect on the heating and cooling energy reductions. However, they also found that the annual total heating and cooling loads were minimized when the phase change temperature of PCM within the outer and inner layers was near the desired indoor temperature.

Mathieu-Potvin and Gosselin [36] conducted a numerical study of south-facing multilayer exterior walls consisting of a plane-parallel PCM layer sandwiched between two insulation layers. First, the effects of the position and phase change temperature of the PCM layer on the annual energy flux through the wall subjected to sinusoidal outdoor temperature oscillations were studied. The annual energy flux was minimized when the PCM layer was positioned near the center of the wall and the phase change temperature was close to the indoor temperature. Second, a genetic algorithm was used to optimize a 20-layer wall to minimize the annual thermal energy flux through the wall subjected either to sinusoidal outdoor temperature boundary conditions or to outdoor temperature and solar radiation heat flux based on real weather data corresponding to Orlando, FL and Quebec City, Canada. Each layer was 0.5 cm thick and was made of concrete, insulation, or pure PCM with one of six possible phase change temperatures. For the wall subjected to sinusoidal outdoor temperature, the optimal design for Quebec City, Canada did not include a PCM layer. The authors postulated that this was because the indoor temperature was not within the range of outdoor temperature variation. However, the optimal design included a PCM layer when the wall was subjected to realistic outdoor temperature and solar radiation heat flux boundary conditions, even though the indoor temperature was not within the range of outdoor temperature variation for most of the year. The authors concluded that realistic outdoor temperature and solar radiation heat flux conditions must be considered in order to determine the energy saving potential of a PCM composite wall.

Hembade et al. [37] simulated transient 1D heat conduction and phase change within a 20 cm thick concrete wall containing a 1–5 cm thick layer of PCM microcapsules over a summer day in Phoenix and Los Angeles. However, it is not clear how the PCM was incorporated into the wall and what method was used to simulate phase change. The wall was subjected to convective heat transfer to a time-dependent indoor temperature varying between 19.9 and 24.9 °C in Phoenix and between 18.9 and 21.9 °C in

Los Angeles. It was also subjected to convective heat transfer to an equivalent outdoor temperature based on weather data. The contribution from solar irradiation on the outer wall was accounted for via the outdoor temperature using the sol–air temperature method, widely used in architecture [38]. The PCM layer was treated as homogeneous having the thermal properties of microencapsulated paraffin but the authors did not account for the thermal properties of the continuous phase (e.g., concrete). Different PCMs were used in each climate with phase change temperature window of 27–31 °C in Phoenix and of 22–25 °C in Los Angeles. The PCM used in Phoenix had a substantially larger density and latent heat of fusion and a smaller thermal conductivity than that used in Los Angeles. The authors found that adding a 5 cm thick (25 vol.%) layer of PCM reduced the daily energy flux through the inner surface of the wall by 60% and 40% in Phoenix and Los Angeles, respectively. The larger reduction in Phoenix can be attributed, in part, to the fact that the sensible and latent heat storage capacity and the thermal resistance were larger for the wall simulated for Phoenix. Unfortunately, it is difficult to draw design rules from these simulations as both the thermal properties of the PCM and the indoor temperature varied in each climate and no systematic parametric or optimization study was performed. In addition, treatment of the solar irradiance on the outer wall surface was not rigorous although essential, according to Mathieu-Potvin and Gosselin [36].

Kissock and Limas [39] solved the transient 1D heat diffusion equation in a 30.4 cm thick multilayer wall consisting of an insulation layer sandwiched between two concrete layers each imbibed with 10 wt.% PCM. The wall was subjected to convective heat transfer to a constant indoor temperature of 21.1 °C and to an outdoor temperature varying sinusoidally between 10 and 32.2 °C over a single day. The density and thermal conductivity of the PCM-concrete composite layers were assumed to be identical to that of pure concrete. The effective specific heat was determined by a weighted average of the concrete specific heat and the temperature-dependent PCM specific heat measured using a differential scanning calorimeter. The authors assumed that the ideal phase change temperature to minimize heat transfer through a wall would be identical to the desired indoor temperature and they shifted the temperature-dependent PCM specific heat accordingly. The maximum heat flux through the wall was reduced by 77% and delayed by 4 h by adding 10 wt.% PCM to the concrete layers. However, directly imbibing concrete with PCM is neither a realistic, nor a durable solution as the PCM reacts chemically with the cement featuring very high pH. Thus, PCM should be microencapsulated, as previously discussed. In addition, in their diurnal simulations, Kissock and Limas [39] ignored (i) heating of the outer wall surface by solar radiation and (ii) the effect of PCM on the effective density and thermal conductivity of the composite wall.

Overall, the literature reported contradictory conclusions about the effects of phase change temperature window ΔT_{pc} on the time-dependent thermal load through multilayer walls containing PCM. Previous studies of microencapsulated PCM-concrete walls [37] did not rigorously account for the thermal effects of the PCM, shell, and/or concrete matrix materials. In addition, no study has performed a systematic parametric analysis to determine design rules to minimize and/or delay the heat transfer rate through such a wall based on climate conditions. The aim of the present study is (1) to develop a simple, efficient, and accurate thermal model of microencapsulated PCM-concrete composite walls and (2) to investigate the impact of adding microencapsulated PCMs to concrete walls on the thermal load of buildings. The effects of four design parameters, namely, (i) the PCM volume fraction, (ii) latent heat of fusion, (iii) phase change temperature and (iv) temperature window on the reduction and delay of thermal load were systematically evaluated, along with the effect of the outdoor temperature oscillations.

3. Analysis

3.1. Schematic

Fig. 1a shows a single unit cell containing core–shell particles arranged in a face-centered cubic (FCC) packing. The corresponding core and shell volume fractions ϕ_c and ϕ_s are respectively expressed as,

$$\phi_c = \frac{2\pi D_c^3}{3a^3} \quad \text{and} \quad \phi_s = \frac{2\pi\left(D_s^3 - D_c^3\right)}{3a^3} \tag{4}$$

where a is the length of the unit cell while D_c and D_s are the inner core and outer shell diameters, respectively. The unit cell width a was arbitrarily taken to be 25 μm for all cases considered. Throughout this study, ϕ_s was arbitrarily imposed to be 8% and D_c and D_s were adjusted based on the desired PCM volume fraction ϕ_c. The volume fraction of core with respect to shell material $\phi_{c/s} = (D_c/D_s)^3$ ranged from about 55% to 86%. This was within a realistic range of microencapsulated PCMs [21]. It was achieved by adjusting D_c and D_s ranging from about 9 to 15 μm and from about 11 to 16 μm, respectively. Note that, in a recent study [40], we showed that the packing arrangement and the polydispersity of the microcapsules had no effect on the effective thermal conductivity of the composite wall. In other words, the situation depicted in Fig. 1a is also representative of the practical situation of randomly distributed and polydisperse microcapsules in concrete [40]. Fig. 1b illustrates a heterogeneous slab of a three-component composite material consisting of aligned unit cells of monodisperse microcapsules filled with PCM and embedded in a concrete matrix in an FCC packing arrangement. It also shows the associated coordinate system and the boundary conditions used to validate the

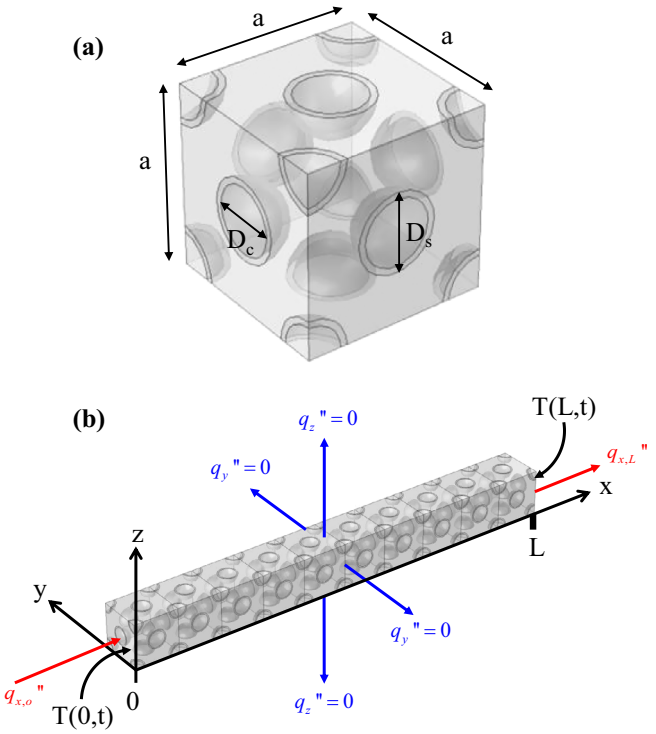

Fig. 1. (a) Schematic of a single unit cell containing core–shell capsules with a face-centered cubic packing arrangement and (b) schematic and coordinate system of a heterogeneous composite of length L made up of aligned unit cells. Core and shell diameters and unit cell length corresponding to core and shell volume fractions ϕ_c and ϕ_s were denoted by D_c, D_s, and a, respectively.

effective homogeneous model. The overall thickness of this composite slab was denoted by L.

3.2. Assumptions

To make the problem mathematically tractable, the following assumptions were made: (1) all materials were isotropic and had constant properties except for the temperature-dependent specific heat of the PCM given by Eq. (3). (2) The specific heat of the PCM was the same for solid and liquid phases, i.e., $c_{p,c,s} = c_{p,c,l}$. (3) Interfacial contact resistances between the concrete, the shell, and the PCM were negligible. (4) Natural convection in the molten microencapsulated PCM was absent based on the fact that the Rayleigh number was very small, and (5) there was no heat generation in the wall.

3.3. Heterogeneous wall simulations

3.3.1. Governing equations

Under the above assumptions, the local temperatures in the PCM, shell, and concrete at time t and location $\mathbf{r} = \langle x, y, z\rangle$ within the heterogeneous composite material denoted by $T_c(\mathbf{r}, t), T_s(\mathbf{r}, t)$, and $T_m(\mathbf{r}, t)$ were governed by the transient heat conduction equation in each domain, given by,

$$\frac{\partial T_c}{\partial t} = \alpha_c(T_c)\nabla^2 T_c, \quad \frac{\partial T_s}{\partial t} = \alpha_s \nabla^2 T_s, \quad \text{and} \quad \frac{\partial T_m}{\partial t} = \alpha_m \nabla^2 T_m \tag{5}$$

where $\alpha_j = k_j/\rho_j c_{p,j}$ is the thermal diffusivity of constituent j, where subscripts "c", "s", and "m" refer to the core, the shell, and the matrix, respectively. Here, the heat capacity method was used to solve for the local temperature $T_c(\mathbf{r}, t)$.

3.3.2. Boundary conditions

These transient three-dimensional (3D) energy conservation equations were solved in the PCM, the shell, and the concrete domains. The initial temperature was assumed to be uniform throughout the composite material and equal to T_i, i.e.,

$$T(x, y, z, 0) = T_i \tag{6}$$

At time $t = 0$, the temperature was imposed on the faces of the slab located at $x = 0$ and $x = L$ so that the overall heat transfer took place along the x-direction (Fig. 1b), i.e.,

$$T(0, y, z, t) = T(0, t) \quad \text{and} \quad T(L, y, z, t) = T(L, t) \tag{7}$$

where $T(0, t)$ and $T(L, t)$ were taken as constant and equal to T_0 and T_L, respectively.

By virtue of symmetry, the heat flux through the four lateral faces vanished, i.e.,

$$q''_y(x, 0, z, t) = q''_y(x, a, z, t) = 0 \ \text{ and } \ q''_z(x, y, 0, t) = q''_z(x, y, a, t) = 0 \tag{8}$$

where $q''_y(x, y, z, t)$ and $q''_z(x, y, z, t)$ are the heat fluxes at location (x, y, z) along the y- and z-axes and given by Fourier's law, i.e., $q''_y = -k\partial T/\partial y$ and $q''_z = -k\partial T/\partial z$, respectively.

Coupling between the temperatures in the different domains of the heterogeneous composite was achieved by imposing continuous heat flux boundary conditions across their interfaces, i.e.,

$$-k_m \left.\frac{\partial T_m}{\partial \mathbf{n}}\right|_{m/s} = -k_s \left.\frac{\partial T_s}{\partial \mathbf{n}}\right|_{m/s} \quad \text{and} \quad -k_s \left.\frac{\partial T_s}{\partial \mathbf{n}}\right|_{s/c} = -k_c \left.\frac{\partial T_c}{\partial \mathbf{n}}\right|_{s/c} \tag{9}$$

where k_m, k_s, and k_c are the thermal conductivities of the matrix, shell, and core, respectively, and $\mathbf{n}$ is the unit normal vector at any given point on the concrete/shell and shell/PCM interfaces, designated by m/s and s/c, respectively.

3.3.3. Constitutive relationships

Table 1 summarizes the thermophysical properties of the different materials used in this study. The density, thermal conductivity, and specific heat of the PCM, shell, and matrix corresponded to those of a commercial organic PCM PureTemp 20 by Entropy Solution Inc. (Plymouth, MN) [41], high density polyethylene (HDPE) [42], and concrete [43], respectively. Here, the PCM specific heat $c_{p,c}(T_c)$ was given by Eq. (3). The phase change temperature T_{pc} and temperature window ΔT_{pc} as well as the latent heat of fusion h_{sf} of the PCM were treated as parameters.

Due to the heterogeneous nature of the composite and to the differences in the thermal properties of the core, shell, and matrix, the heat flux was not necessarily uniform over a given cross-section perpendicular to the x-axis. Thus, the area-averaged heat flux $\bar{q}''_x$ along the x-direction was defined as,

$$\bar{q}''_x(x, t) = \frac{1}{A_c}\iint q''_x(x, y, z, t)\,dy\,dz \tag{10}$$

where A_c is the cross-sectional area of the computational domain perpendicular to the x-axis.

3.4. Homogeneous wall simulations

3.4.1. Governing equation

The temperature T in the homogeneous material equivalent to the heterogeneous wall of identical dimensions was governed by

$$\frac{\partial T}{\partial t} = \alpha_{eff}(T)\nabla^2 T \tag{11}$$

where $\alpha_{eff}(T) = k_{eff}/(\rho c_p)_{eff}(T)$ is the effective thermal diffusivity. Note that $\alpha_{eff}(T)$ is a function of the local temperature T since it accounts for the temperature-dependent specific heat of the PCM. However, a consistent model for the effective volumetric heat capacity $(\rho c_p)_{eff}$ and the effective thermal conductivity k_{eff} of the composite wall needs to be specified.

3.4.2. Effective thermal properties

To approximate the heterogeneous composite by a homogeneous medium with some effective thermal properties, it is necessary to define its effective volumetric heat capacity $(\rho c_p)_{eff}$ and its effective thermal conductivity k_{eff}. First, from thermodynamic considerations, the volumetric heat capacity of any material (ρc_p) is related to its enthalpy H according to [44],

$$\rho c_p V = \frac{\partial H}{\partial T} \tag{12}$$

where V is the volume of the material. Eq. (12) applies not only to single phase systems but also to a three-component composite wall of total volume $V_t = V_c + V_s + V_m$ where V_c, V_s, and V_m are the overall volumes occupied by the core, shell, and matrix, respectively. The corresponding total enthalpy H_t (in J) is the sum of the enthalpies of each constituent, i.e., $H_t = H_c + H_s + H_m$. Thus, the effective volumetric heat capacity can be expressed as,

$$(\rho c_p)_{eff}(T) = \frac{1}{V_t}\frac{\partial H_t}{\partial T} = \phi_c(\rho c_p)_c(T) + \phi_s(\rho c_p)_s + (1 - \phi_c - \phi_s)(\rho c_p)_m \tag{13}$$

where $\phi_c = V_c/V_t$ and $\phi_s = V_s/V_t$ are the volume fractions of the core and shell materials, while $(\rho c_p)_c$, $(\rho c_p)_s$, and $(\rho c_p)_m$ are the

Table 1
Density ρ, specific heat capacity c_p, and thermal conductivity k of PCM, high density polyethylene (HDPE), and concrete.

Material	Subscript	ρ (kg/m^3)	c_p (J/kg K)	k (W/m K)	Refs.
PCM	c	860	2590	0.21	[41]
HDPE	s	930	2250	0.49	[42]
Concrete	m	2300	880	1.4	[43]

volumetric heat capacities of the core, shell, and matrix materials, respectively. By substituting $c_{p,c}(T)$ given by Eq. (3) into Eq. (13), $(\rho c_p)_{eff}(T)$ can be expressed as,

$$(\rho c_p)_{eff}(T) = \begin{cases} (\rho c_p)_{eff,s} & \text{for} \quad T < T_{pc} - \Delta T_{pc}/2 \\ (\rho c_p)_{eff,s} + \phi_c \frac{\rho_c h_{sf}}{\Delta T_{pc}} & \text{for} \quad T_{pc} - \Delta T_{pc}/2 \leqslant T \leqslant T_{pc} + \Delta T_{pc}/2 \\ (\rho c_p)_{eff,l} & \text{for} \quad T > T_{pc} + \Delta T_{pc}/2 \end{cases} \tag{14}$$

where $(\rho c_p)_{eff,s}$ is the effective volumetric heat capacity of the PCM-concrete composite wall with unmelted PCM given by $(\rho c_p)_{eff,s} = \phi_c(\rho c_p)_{c,s} + \phi_s(\rho c_p)_s + (1-\phi_c-\phi_s)(\rho c_p)_m$. Here, it was assumed to be equal to the effective volumetric heat capacity of the composite with fully melted PCM, i.e., $(\rho c_p)_{eff,s} = (\rho c_p)_{eff,l}$.

Moreover, Felske [45] used the self-consistent field approximation [46] to derive an effective medium approximation (EMA) to predict the effective thermal conductivity k_{eff} of monodisperse spherical capsules randomly distributed in a continuous matrix given by,

$$k_{eff} = \frac{2k_m(1-\phi_c-\phi_s)\left(3+2\frac{\phi_s}{\phi_c}+\frac{\phi_s k_c}{\phi_c k_s}\right)+(1+2\phi_c+2\phi_s)\left[\left(3+\frac{\phi_s}{\phi_c}\right)k_c+2\frac{\phi_s k_s}{\phi_c}\right]}{(2+\phi_c+\phi_s)\left(3+2\frac{\phi_s}{\phi_c}+\frac{\phi_s k_c}{\phi_c k_s}\right)+(1-\phi_c-\phi_s)\left[\left(3+\frac{\phi_s}{\phi_c}\right)\frac{k_c}{k_m}+2\frac{\phi_s k_s}{\phi_c k_m}\right]}. \tag{15}$$

This expression was validated using detailed numerical simulations of ordered and randomly distributed monodisperse and polydisperse microcapsules [40].

It is important to note that Eqs. (13)–(15) indicate that the effective volumetric heat capacity and thermal conductivity depended only on the constitutive phase properties and on their volume fractions. They were independent of core and shell diameters, microcapsule spatial arrangement, and polydispersity. Thus, from a thermal point of view, FCC packing is representative of any arbitrary packing arrangement, as previously discussed [40].

3.4.3. Boundary conditions

Two types of boundary conditions were imposed on the homogeneous wall. First, to demonstrate that the heterogeneous composite can be treated as a homogeneous material with some effective thermal properties, the initial and boundary conditions given by Eqs. (6) and (7) were imposed with $T(0,t) = T_0$ and $T(L,t) = T_L$. Second, when simulating sinusoidal diurnal boundary conditions, convective heat transfer was imposed at the interior wall surface $x = L$ with a constant indoor temperature T_{in} maintained by the HVAC system so that [36],

$$-k_{eff}\frac{\partial T}{\partial x}(L,y,z,t) = h_i[T(L,t) - T_{in}] \tag{16}$$

where h_i is the indoor mixed convective heat transfer coefficient accounting for both forced and natural convections. Combined convective and radiative heat transfer was imposed at the exterior wall surface given by Mathieu-Potvin and Gosselin [36] and Diaconu and Cruceru [35],

$$-k_{eff}\frac{\partial T}{\partial x}(0,y,z,t) = h_o[T(0,t) - T_\infty(t)] + \alpha_s q''_s(t) - \epsilon\sigma[T(0,t)^4 - T_{sky}^4] \tag{17}$$

where h_o is the outdoor convective heat transfer coefficient, T_{sky} represents the average sky temperature, α_s and ϵ are the total hemispherical absorptivity and emissivity of the outdoor wall surface, respectively, and σ is the Stefan–Boltzmann constant, i.e., $\sigma = 5.67 \times 10^{-8}$ W/m^2 K^4. The ambient outdoor temperature $T_\infty(t)$ was imposed as a sinusoidal function of time t (in s) expressed as,

$$T_\infty(t) = \frac{T_{max}+T_{min}}{2} + \frac{T_{max}-T_{min}}{2}\sin\left(\frac{\pi}{43,200}t - \frac{2\pi}{3}\right) \tag{18}$$

where T_{max} and T_{min} are the maximum and minimum outdoor temperatures during a day, respectively. A phase shift of $2\pi/3$ placed the peak outdoor temperature T_{max} at 2:00 pm, as the daily maximum occurred between 1:00 pm and 3:00 pm for more than 80% of the year in California climate zone 9 (Los Angeles, CA) based on weather data [47]. Similarly, the solar radiation heat flux $q''_s(t)$ as a function of time t (in s) was imposed as,

$$q''_s(t) = \begin{cases} 0 & \text{for} \quad 6:00\text{ pm} \leqslant t \leqslant 6:00\text{ am} \\ q''_{s,max}\cos\left(\frac{\pi}{43,200}t - \pi\right) & \text{for} \quad 6:00\text{ am} \leqslant t \leqslant 6:00\text{ pm} \end{cases} \tag{19}$$

where $q''_{s,max}$ is the maximum daily solar radiation heat flux (in W/m^2). Here, the maximum daily solar radiation heat flux $q''_{s,max}$ was taken as 535 W/m^2 and occurred at 12:00 pm corresponding to the average daily maximum value and time throughout the year in California climate zone 9 [47].

3.4.4. Constitutive relationships

The indoor heat transfer coefficient h_i was taken to be 8 W/m^2 K. This value was consistent with experimental measurements for mixed forced and natural convection on a vertical wall reported by Awbi and Hatton [48]. The outdoor heat transfer coefficient h_o was taken as 20 W/m^2 K, based on previous numerical simulations of walls exposed to outdoor weather conditions [37,49]. These values of indoor h_i and outdoor h_o heat transfer coefficients were very similar to those recommended by ISO standard 6946 of 7.7 and 25 W/m^2 K, respectively [50]. The total hemispherical solar absorptivity α_s and surface emissivity ϵ of the outer wall were taken as 0.26 and 0.9, respectively corresponding to typical values for white paint [43]. Finally, an average sky temperature T_{sky} of 2 °C was used [43]. Four outdoor temperature conditions were considered with minimum and maximum outdoor temperatures T_{min} and T_{max} set at (i) 20 and 40 °C, (ii) 10 and 30 °C, (iii) 0 and 20 °C, or (iv) 5 and 35 °C, respectively. Table 1 summarizes the properties corresponding to PureTemp 20 PCM microencapsulated in HDPE and dispersed in concrete. The resulting effective volumetric heat capacity $(\rho c_p(T))_{eff}$ increased and the effective thermal conductivity k_{eff} decreased nearly linearly with increasing PCM volume fraction ϕ_c from 0.0 to 0.5 and $\phi_s = 0.08$ (see Supplementary material). Thus, both the thermal resistance and the sensible heat storage capacity of the composite wall increased with the addition of PCM.

3.5. Performance metrics

Many numerical studies considering building materials containing PCMs reported either the inside surface temperature of the wall and/or the average indoor temperature [31,33,51]. It has been suggested that reducing the fluctuation of these temperatures enhances the thermal comfort of occupants within a room [31,33]. However, they do not directly contribute in determining energy or cost savings. In the present study, the energy flux reduction and the time delay of the maximum thermal load were used to evaluate the performance of PCM composite walls with respect to plain concrete walls. First, the energy flux reduction E_r was defined as the relative difference between the daily energy fluxes (in J/m^2) through the plain concrete wall $Q''_{L,m}$ and through the PCM-concrete composite wall Q''_L expressed as,

$$E_r = \frac{Q''_{L,m} - Q''_L}{Q''_{L,m}} \tag{20}$$

where the energy fluxes $Q''_{L,m}$ and Q''_L were respectively expressed as,

$$Q''_{L,m} = \int_0^{24\ h} |q''_{L,m}(t)|dt \quad \text{and} \quad Q''_L = \int_0^{24\ h} |q''_L(t)|dt \tag{21}$$

Here, $q''_{L,m}$ and q''_L are the conductive heat fluxes (in W/m^2) at the inner wall located at $x = L$ for plain concrete walls and for PCM-concrete composite walls, respectively. They are given by Fourier's law as,

$$q''_{L,m}(t) = -k_m \left.\frac{\partial T_m}{\partial x}\right|_L \quad \text{and} \quad q''_L(t) = -k_{eff} \left.\frac{\partial T}{\partial x}\right|_L \tag{22}$$

The absolute values of $q''_{L,m}$ and q''_L were considered to account for the fact that there is an energy cost associated with maintaining the indoor temperature at T_{in}, regardless of the direction of the heat flux across the wall. The energy flux reduction E_r describes the reduction in the daily thermal energy added or removed from the room per unit surface area of wall achieved by adding microencapsulated PCM to the concrete wall.

The second performance metric considered was the time delay τ_d of the maximum inner wall heat flux defined as $\tau_d = t_{max} - t_{max,m}$ where t_{max} and $t_{max,m}$ are the times at which $q''_L(t)$, for the PCM-concrete composite wall, and $q''_{L,m}(t)$, for the plain concrete wall, reached their respective maximum value during the day. The time delay is an important metric when a building is located in a place, such as California, where TOU electricity rate schedules are used by utility companies. In these cases, the time delay of the heat flux may shift the peak cooling load to a time of day with lower electricity rates, thus resulting in cost savings for the ratepayer.

3.6. Method of solution

The governing Eqs. (5) and (11) along with the initial and boundary conditions given by Eqs. (6)–(9), (16), and (17) were solved using the commercial finite element solver COMSOL Multiphysics 4.3. In cases with varying outdoor boundary temperatures, simulations were run for 3 days and temperature and heat flux predictions for the third day were considered. By then, the diurnal heat flux had reached periodic steady-state and the maximum relative difference in the inner wall heat flux was less than 1% when extending the simulation period by one day. Numerical convergence was considered to be achieved if the maximum relative difference in the predicted local heat flux $q''_x(x,t)$ was less than 0.5% when reducing the mesh size or time step by a factor of 2. In practice, converged solutions were obtained by imposing the minimum mesh size and maximum growth rate to be $\Delta x = (D_s - D_c)/6$ and 1.5, respectively. The number of finite elements needed to obtain a converged solution ranged from 3289 to 786,985 depending on the size of the computational cell and on the core and shell dimensions.

3.7. Validation

In order to validate the computational tool, heat conduction through a two-dimensional 0.1×0.2 m^2 rectangular paraffin slab heated at constant temperature on one side and thermally insulated on the other. This slab, undergoing partial solid–liquid phase transition was simulated following the study by Ogoh and Groulx [30]. The predicted transient temperature profiles agreed well with the exact solution for the one-dimensional Stefan problem derived by Alexiades [52] (see Supplementary material). The results were also consistent with those of Ogoh and Groulx [30] and support their conclusion that conduction through a material during phase change can be modeled numerically using the heat capacity method.

4. Results and discussion

4.1. Heterogeneous vs. homogeneous wall

In this section, we consider the slab of heterogeneous composite material shown in Fig. 1b with thickness $L = 1$ mm subjected to a step boundary condition given by Eqs. (6) and (7). The initial temperature T_i and inner surface temperature $T(L,t) = T_L$ were equal and arbitrarily chosen to be 20 °C, and the outer surface temperature $T(0,t) = T_0$ was taken as 37 °C. The composite material consisted of PCM microencapsulated in HDPE shells and distributed in concrete (Table 1) and featured PCM volume fractions ϕ_c of 0.05, 0.25, or 0.40 while ϕ_s was constant and equal to 0.08. The corresponding effective volumetric heat capacity $(\rho c_p)_{eff,s}$ of the equivalent homogeneous wall predicted by Eq. (13) was 2.04, 2.08, and 2.11 MJ/m^3 K, respectively. Similarly, the effective thermal conductivity k_{eff} predicted by Eq. (15) was 1.23, 0.94, and 0.75 W/m K, respectively. The latent heat of fusion h_{sf}, phase change temperature T_{pc}, and temperature window ΔT_{pc} of the PCM were taken as 180 kJ/kg, 21.5 °C, and 3 °C, respectively.

Fig. 2 shows the area-averaged inner surface heat flux $\bar{q}''_L(t) = q''_x(L,t)$ as a function of time for PCM volume fraction ϕ_c of 0.5, 0.25, and 0.4. It also shows the corresponding predictions of the heat flux for the equivalent homogeneous slab with the above mentioned effective thermal properties. In all cases, the average relative difference in the predicted area-averaged inner surface heat flux $\bar{q}''_L(t)$ between the heterogeneous composite slab and the equivalent homogeneous slab was less than 2% at all times when the inner surface heat flux was greater than 5% of its steady-state value. Fig. 2 also demonstrates that increasing the PCM volume fraction decreased the inner surface heat flux at all times and delayed its steady state. This can be attributed to the fact that adding PCM not only enhanced the latent and sensible thermal mass of the composite material but also its thermal resistance.

Fig. 3 compares the temperature profiles along the centerline $(x, a/2, a/2)$ of the composite structure of Fig. 1b at different times predicted for the heterogeneous composite and for the corresponding homogeneous material for (a) $\phi_c = 0.05$ and (b) $\phi_c = 0.40$ under the same conditions as the results shown in Fig. 2. The relative difference in the local temperature between the heterogeneous composite and the equivalent homogeneous material was

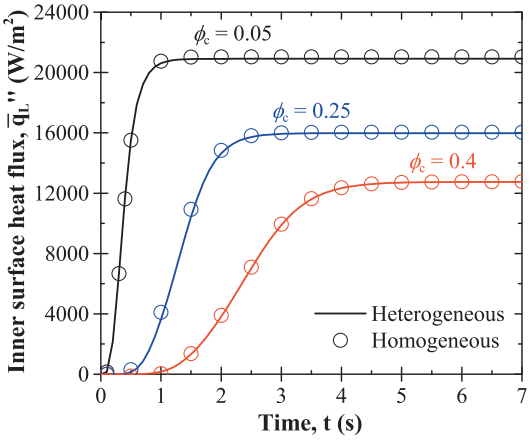

Fig. 2. Area-averaged inner surface heat flux $\bar{q}''_L$ predicted for the heterogeneous three-phase 1 mm thick slab and the corresponding homogeneous slab with effective thermal properties as a function of time t for $T(0,t) = T_0 = 20$ °C and $T(L,T) = T_L = 37$ °C. Values of effective volumetric specific heat and effective thermal conductivity were $(\rho c_p)_{eff,s} = 2.04$, 2.08, and 2.11 MJ/m^3 K and $k_{eff} = 1.23$, 0.94, and 0.75 W/m K corresponding to PCM volume fractions of $\phi_c = 0.05$, 0.25, and 0.4, respectively. The phase change properties were taken to be $h_{sf} = 180$ kJ/kg, $T_{pc} = 20$ °C, and $\Delta T_{pc} = 3$ °C.

less than 1% at all times and locations. Fig. 3a and b confirm that the time delay in the temperature evolution increased with increasing PCM volume fraction. They also illustrate that the temperature front progressed faster in the absence of phase change.

Overall, these results demonstrated that the heterogeneous composite can be treated as a homogeneous material with effective volumetric heat capacity $(\rho c_p)_{eff}(T)$ and effective thermal conductivity k_{eff} given by Eqs. (13)–(15). Consequently, for the remainder of this study, a PCM-concrete composite wall will be simulated as a homogeneous wall with these effective thermal properties. This will make possible the simulation of walls with realistic thickness L, on the order of tens of centimeters. Simulating a heterogeneous wall of such thickness with PCM microcapsules would be excessively time consuming and would require large computational resources due to the large number of mesh elements required to solve for the local temperature in the PCM and shell of the microcapsules.

4.2. Diurnal thermal behavior

4.2.1. Effect of PCM volume fraction

This section considered homogeneous walls of thickness $L = 10$ cm subjected to sinusoidal diurnal boundary conditions imposed at the inner and outer wall surfaces as described by Eqs. (16)–(19). The latent heat of fusion h_{sf}, phase change temperature T_{pc}, and temperature window ΔT_{pc} were taken as 180 kJ/kg, 20 °C, and 3 °C, respectively. The outdoor temperature $T_\infty(t)$ described by Eq. (18) oscillated sinusoidally around T_{pc} between $T_{min} = 10$ °C and $T_{max} = 30$ °C. In order to isolate the thermal effect of varying the PCM volume fraction ϕ_c, the shell volume fraction ϕ_s was taken as constant and equal to 0.08, representative of actual commercial products [41]. Note that the trends and design rules reported in this paper were found to be the same for different shell volume fractions ϕ_s (not shown). Fig. 4a plots the inner wall heat flux as a function of time for PCM volume fractions ϕ_c ranging from 0.0 to 0.5. It demonstrates that increasing the PCM volume fraction significantly reduced the heat transfer through the wall. In fact, a PCM volume fraction ϕ_c of 0.5 reduced the range of variation in the inner wall heat flux by more than 90% compared with plain concrete. Moreover, adding microencapsulated PCM to concrete delayed the peak inner wall heat flux corresponding to the maximum cooling load.

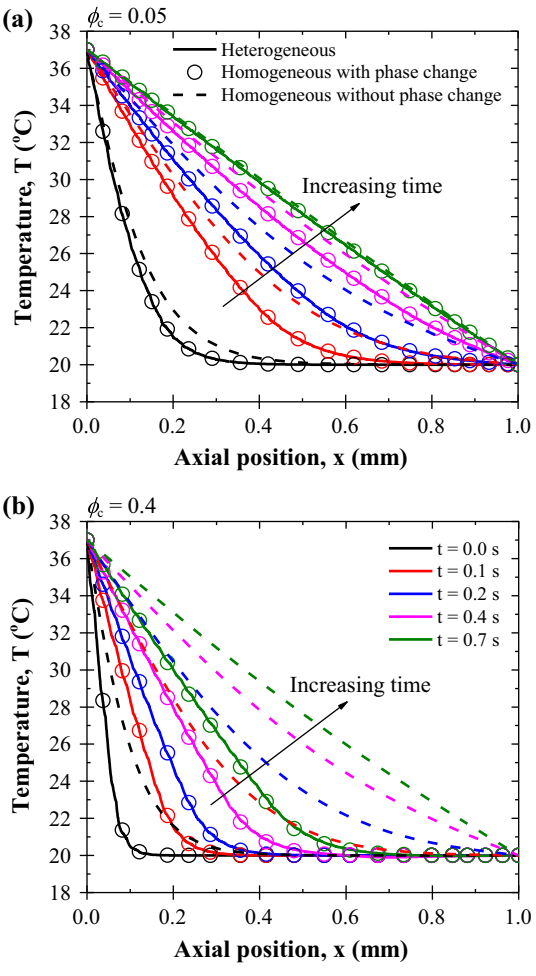

Fig. 3. Temperature profiles at different times through a 1 mm thick heterogeneous composite slab and its equivalent homogeneous slab with and without phase change for PCM volume fraction of (a) $\phi_c = 0.05$ and (b) $\phi_c = 0.4$, respectively. All boundary conditions and thermal properties were consistent with those specified for Fig. 2.

Fig. 4b plots the energy flux reduction E_r as a function of PCM volume fraction ϕ_c ranging from 0.0 to 0.5. In order to distinguish the contribution of phase change from that of other thermal effects, the PCM specific heat $c_{p,c}$ was imposed to be either constant and equal to $c_{p,c,s}$ or a function of temperature as described by Eq. (3). Fig. 4b shows that the energy flux reduction E_r increased substantially with increasing PCM volume fraction. In the absence of phase change, E_r increased linearly with increasing ϕ_c due to the associated increase in thermal resistance and sensible heat storage of the wall, i.e., $k_{eff} < k_m$ and $(\rho c_p)_{eff,s} > (\rho c_p)_m$. The energy flux reduction E_r was notably larger when phase change was accounted for. However, its rise slowed down significantly when the PCM volume fraction ϕ_c exceeded 0.2. In fact, the temperature profile corresponding to $\phi_c = 0.5$ revealed that the temperature within a portion of the wall never exceeded the upper limit of the phase change temperature window $T_{pc} + \Delta T_{pc}/2$ during the day. In other words, the benefit of the latent heat of fusion was not fully realized when the PCM volume fraction exceeded a critical value.

Fig. 4c shows the time delay τ_d in the maximum inner wall heat flux as a function of PCM volume fraction ϕ_c. It indicates that τ_d increased significantly with increasing PCM volume fraction, reaching more than 13 h for ϕ_c of 0.5. Here also, the contribution of phase change to the time delay was important and dominated over that of other thermal effects.

4.2.2. Effect of latent heat of fusion

The inner wall heat flux was computed as a function of time for latent heat of fusion h_{sf} ranging from 100 to 400 kJ/kg, representative of actual PCMs [16,22,41] (see Supplementary material). The volume fraction of PCM ϕ_c, phase change temperature T_{pc}, and temperature window ΔT_{pc} were taken as 0.1, 20 °C, and 3 °C, respectively. The minimum and maximum outdoor temperatures were $T_{min} = 10$ °C and $T_{max} = 30$ °C, respectively. The results established that increasing the latent heat of fusion reduced and delayed heat transfer through the wall. In fact, the energy flux reduction E_r increased from 25% to 64% and the time delay τ_d increased from 0.8 to 5.7 h as h_{sf} increased from 100 to 400 kJ/kg (see Supplementary material). This trend was consistent with physical intuition based on the fact that increasing the latent heat of fusion enhanced the wall's thermal mass and the amount of energy stored therein.

4.2.3. Effect of phase change temperature window

Fig. 5a–c plot the inner wall heat flux $q''_L(t)$ as a function of time for phase change temperature window ΔT_{pc} ranging from 1 to 5 °C and for average outdoor temperature $(T_{max} + T_{min})/2$ of 10, 20, and 30 °C, respectively. The volume fraction of PCM ϕ_c, latent heat of fusion h_{sf}, phase change temperature T_{pc}, and amplitude of the outdoor temperature oscillations $(T_{max} - T_{min})/2$ were taken as 0.1, 180 kJ/kg, 20 °C, and 10 °C, respectively. Fig. 5a indicates that, for

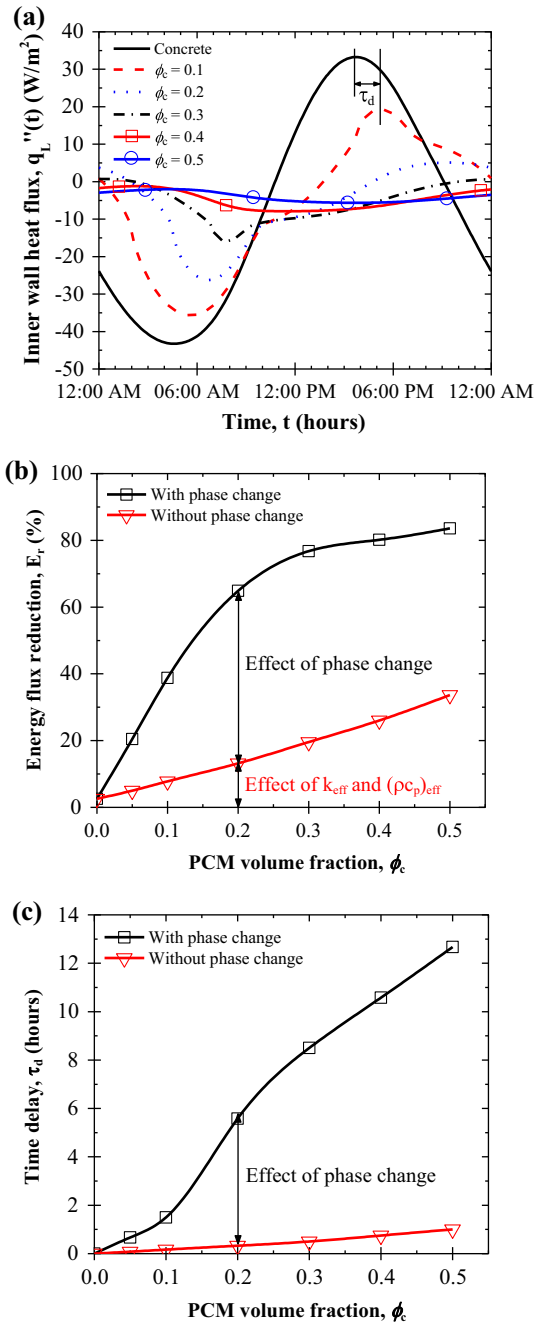

Fig. 4. (a) Inner wall heat flux $q_L''(t)$ as a function of time through a 10 cm thick microencapsulated PCM-concrete wall subjected to sinusoidal diurnal boundary conditions with $T_{min} = 10\,^{\circ}C$ and $T_{max} = 30\,^{\circ}C$. (b) Energy flux reduction E_r and (c) time delay τ_d for PCM volume fraction ϕ_c ranging from 0.0 to 0.5. Here, $h_{sf} = 180$ kJ/kg, $T_{pc} = 20\,^{\circ}C$, and $\Delta T_{pc} = 3\,^{\circ}C$. The PCM specific heat was either constant and equal to $(\rho c_p)_{eff,s}$ or temperature-dependent as defined by Eq. (3) to assess the effects of phase change.

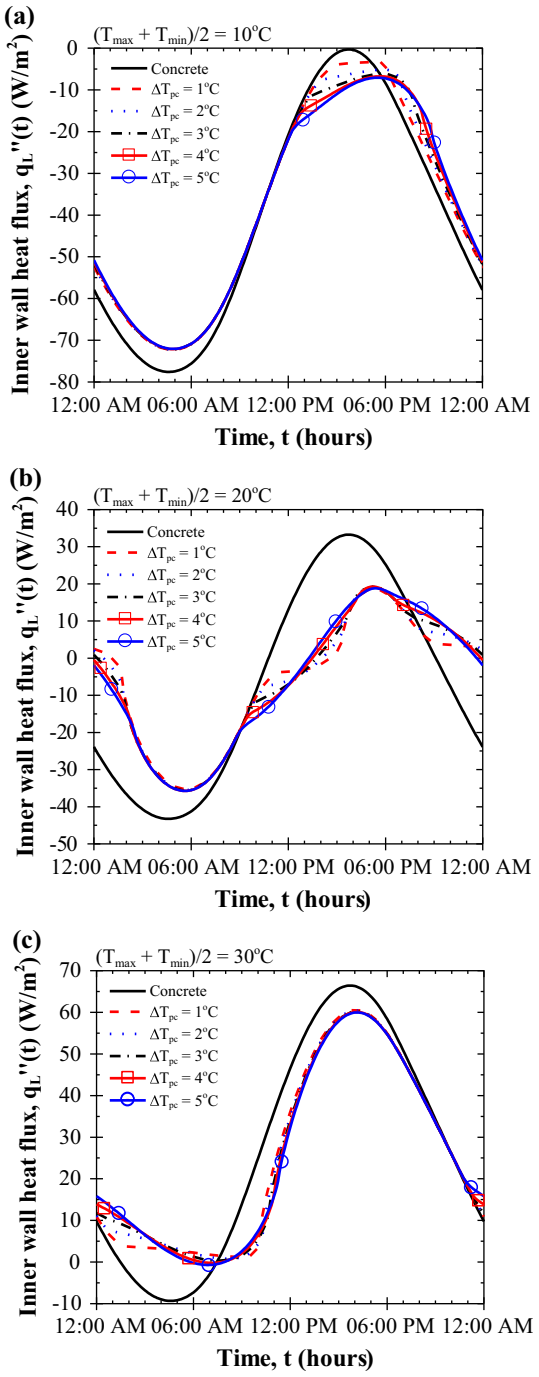

Fig. 5. Inner wall heat flux $q_L''(t)$ as a function of time through a 10 cm thick microencapsulated PCM-concrete wall for ΔT_{pc} ranging from 1 to 5 °C with minimum and maximum outdoor temperatures T_{min} and T_{max} of (a) 0 and 20 °C, (b) 10 and 30 °C, and (c) 20 and 40 °C. Here, $\phi_c = 0.1$, $h_{sf} = 180$ kJ/kg, and $T_{pc} = 20\,^{\circ}C$.

an average daily outdoor temperature $(T_{max} + T_{min})/2$ of 10 °C, changing the phase change temperature window affected only slightly the delay and reduction of heat transfer during the afternoon and evening. The PCM remained solid throughout the wall until the afternoon when the outdoor temperature T_∞ approached the phase change temperature $T_{pc} = 20\,^{\circ}C$. At this time, the wall experienced partial melting, thus reducing and delaying the heat flux. Fig. 5b indicates that, for $(T_{max} + T_{min})/2 = 20\,^{\circ}C$, decreasing ΔT_{pc} from 5 to 1 °C flattened the heat flux curves corresponding to a melting period between 9:00 am and 4:00 pm and a freezing period from 6:00 pm to 2:00 am. However, the minimum and maximum values of the wall heat flux were not affected by changes in ΔT_{pc}. Finally, Fig. 5c illustrates that, for $(T_{max} + T_{min})/2 = 30\,^{\circ}C$, the phase change temperature window had an effect on the delay and reduction in the wall heat flux only during the morning hours. Here, the PCM remained liquid across the wall most of the day except early in the morning when it experienced partial freezing (see Supplementary material).

Moreover, the phase change temperature window ΔT_{pc} was found to have nearly no effects on the energy flux reduction E_r

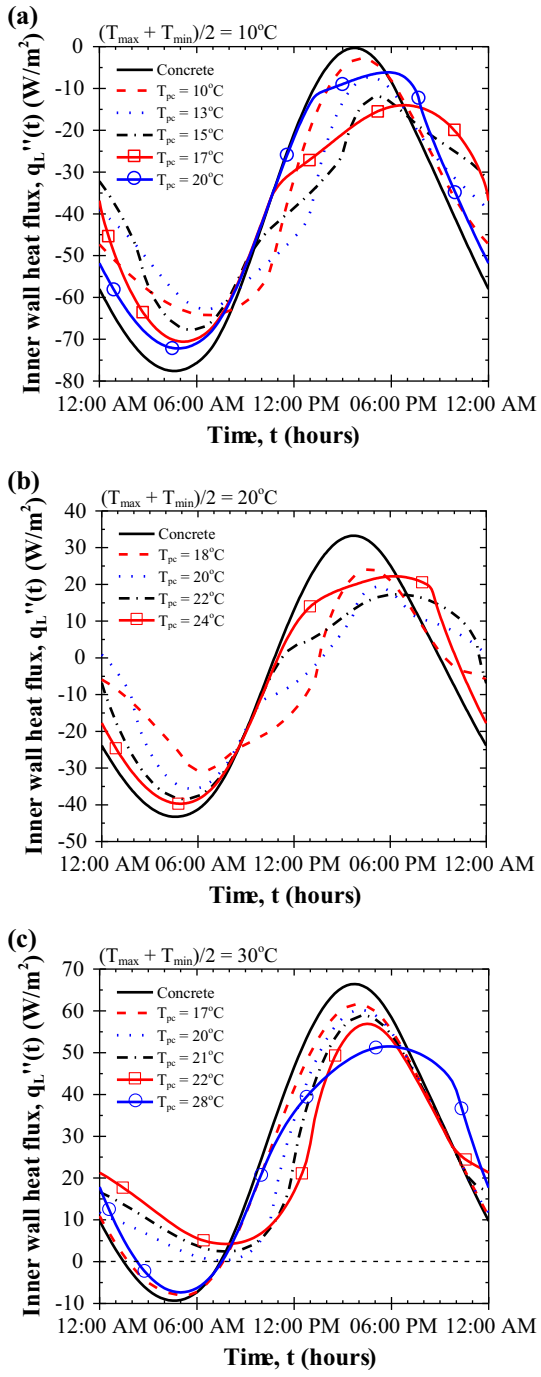

Fig. 6. Inner wall heat flux $q_L''(t)$ as a function of time through a 10 cm microencapsulated PCM-concrete wall for T_{pc} ranging from 10 to 28 °C with minimum and maximum outdoor temperatures T_{min} and T_{max} of (a) 0 and 20 °C, (b) 10 and 30 °C, and (c) 20 and 40 °C, respectively. Here, $\phi_c = 0.1, h_{sf} = 180$ kJ/kg, and $\Delta T_{pc} = 3$ °C.

and on the time delay τ_d. In fact, E_r was strictly independent of ΔT_{pc} when the heat flux was unidirectional during the entire day. Both E_r and τ_d were the largest for $(T_{max} + T_{min})/2$ of 20 °C and equal to ~40% and ~2 h, respectively (see Supplementary material).

4.2.4. Effect of phase change temperature

Fig. 6a–c plot the inner wall heat flux $q_L''(t)$ as a function of time for different phase change temperature T_{pc} ranging from 10 to 28 °C and for average outdoor temperature $(T_{max} + T_{min})/2$ of 10, 20, and 30 °C, respectively. The volume fraction of PCM ϕ_c, latent heat of

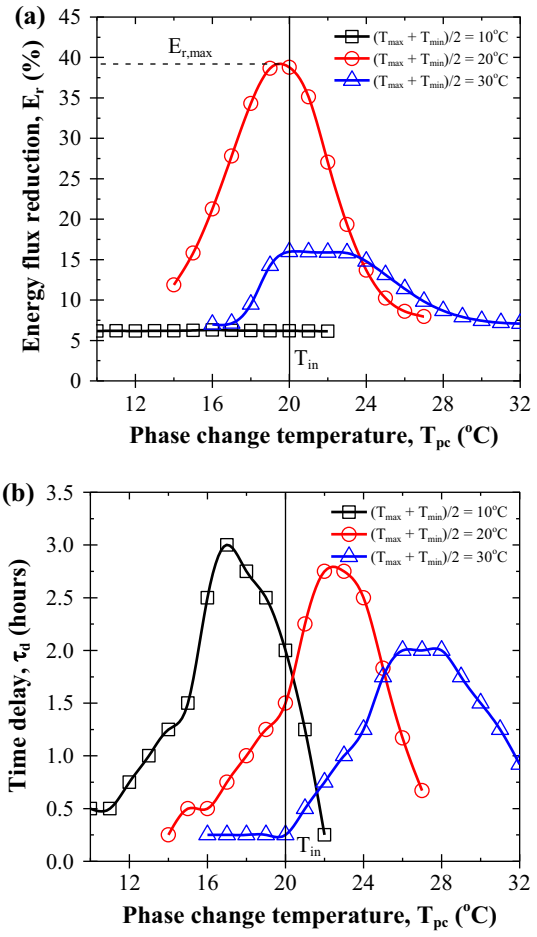

Fig. 7. (a) Energy flux reduction E_r and (b) time delay τ_d as a function of phase change temperature T_{pc} for average outdoor temperature $(T_{max} + T_{min})/2$ of 10, 20, and 30 °C and outdoor temperature amplitude $(T_{max} - T_{min})/2$ of 10 °C. Here, $\phi_c = 0.1, h_{sf} = 180$ kJ/kg, and $\Delta T_{pc} = 3$ °C.

fusion h_{sf}, phase change temperature window ΔT_{pc}, and amplitude of the outdoor temperature oscillations $(T_{max} - T_{min})/2$ were taken as 0.1, 180 kJ/kg, 3 °C, and 10 °C, respectively. Fig. 6a–c indicate that, for given outdoor temperature conditions, increasing the phase change temperature T_{pc} up to a certain value delayed the peak and reduced the amplitude of the heat flux through the micro-encapsulated PCM-concrete composite wall compared with a plain concrete wall. They suggest that the delay and reduction of the thermal load on the wall may be maximized by choosing the optimum phase change temperature based on outdoor temperature conditions.

Fig. 7a plots the energy flux reduction E_r as a function of phase change temperature T_{pc} for average outdoor temperature $(T_{max} + T_{min})/2$ of 10, 20, and 30 °C and for $\phi_c = 0.1, h_{sf} = 180$ kJ/kg, and $\Delta T_{pc} = 3$ °C. First, it is interesting to note that, for an average daily outdoor temperature of 10 °C, even though the shape of the heat flux curves varied dramatically (Fig. 6a), the energy flux reduction was independent of T_{pc}. In fact, the value of E_r was equal to that achieved in the absence of phase change, i.e., energy saving was solely due to the increase in sensible heat storage and thermal resistance. Here, the heat flux was unidirectional from the inside to the outside (i.e., $q_L'' < 0$) throughout the day (Fig. 6a). For an average outdoor temperature of 20 °C, a distinct maximum energy flux reduction $E_{r,max}$ of 39% was achieved for a phase change temperature T_{pc} equal to the indoor temperature T_{in} of 20 °C. This result was consistent with conclusions reported in the literature for multilayer composite walls containing a PCM layer [36,35]. Lastly, for an average

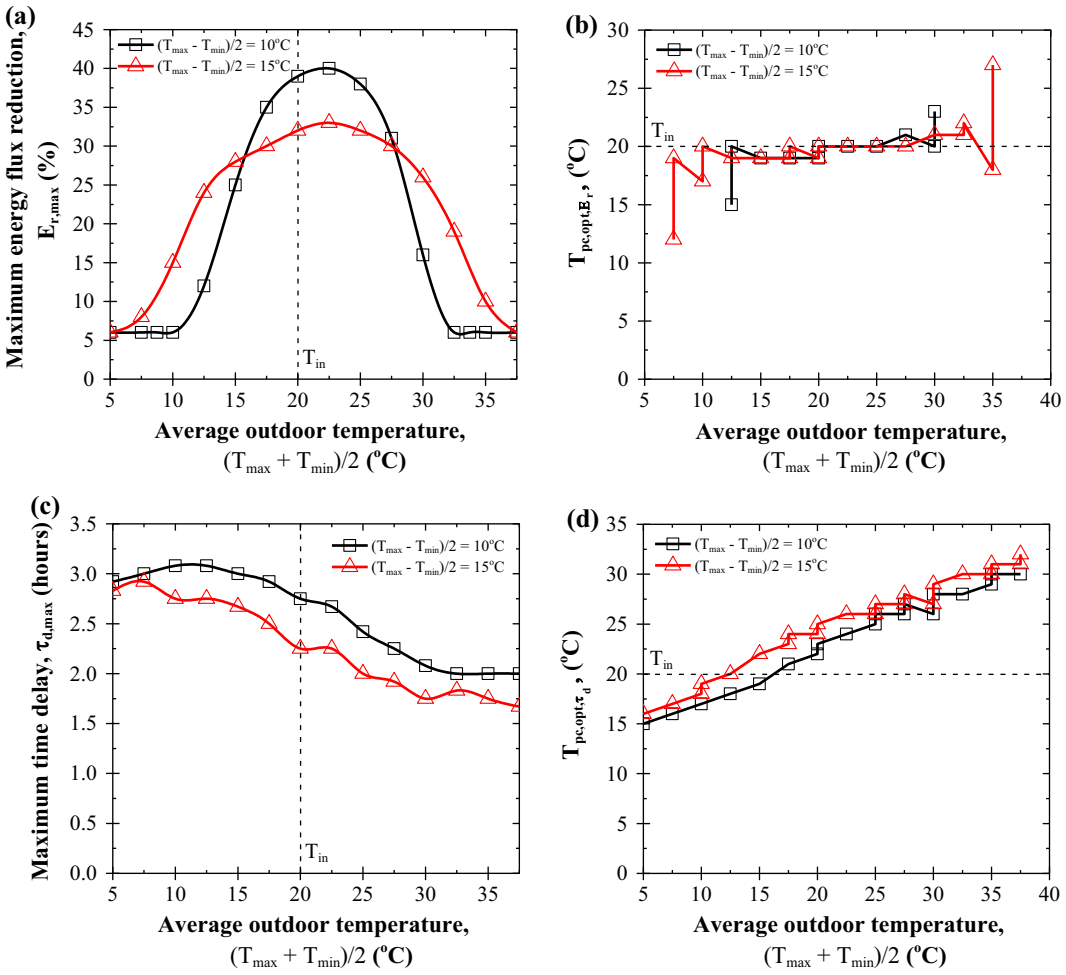

Fig. 8. (a) Maximum energy flux reduction $E_{r,max}$, (b) phase change temperature corresponding to the maximum energy flux reduction T_{pc,opt,E_r}, (c) maximum time delay $\tau_{d,max}$, and (d) phase change temperature corresponding to the maximum time delay T_{pc,opt,τ_d} for average outdoor temperatures ranging from 5 to 37.5 °C with an amplitude of either 10 or 15 °C. Here, $\phi_c = 0.1, h_{sf} = 180$ kJ/kg, and $\Delta T_{pc} = 3$ °C.

outdoor temperature of 30 °C, the energy flux reduction E_r was also independent of the phase change temperature T_{pc} when the latter was either below 17 °C, or above 31 °C. In fact, it was identical to that obtained for $(T_{max} + T_{min})/2 = 10$ °C. For T_{pc} below 17 °C, no phase change occurred since the PCM was liquid for the entire day. When T_{pc} was between 31 and 40 °C, phase change occurred but the heat flux was only reduced and delayed in the afternoon when heat "flowed" into the building. In other words, the heat flux was unidirectional for the duration of the phase change cycle. The energy flux reduction E_r also featured a plateau when T_{pc} was between 20 and 23 °C. Here, the PCM experienced phase transition, but the heat flux was unidirectional throughout the day and E_r was independent of T_{pc}. For other values of T_{pc}, the heat flux through the wall changed direction during the day and the energy flux reduction depended on the phase change temperature. Overall, these results showed that there were no optimization opportunities in terms of energy reduction for a homogeneous PCM composite wall subjected to sinusoidal outdoor temperature oscillations and solar radiation heat flux when the heat flux at the inner wall surface was unidirectional during the entire diurnal cycle. Such situations can be encountered in extremely hot or cold climates.

Fig. 7b plots the time delay τ_d as a function of phase change temperature T_{pc} corresponding to the heat flux shown in Fig. 6 for $\phi_c = 0.1, h_{sf} = 180$ kJ/kg, and $\Delta T_{pc} = 3$ °C. In all cases, τ_d reached a maximum ranging from 2 to 3 h as the average outdoor temperature decreased from 30 to 10 °C. The value of T_{pc} corresponding to the maximum value of τ_d increased with increasing average outdoor temperature. Although there was no optimization opportunity in terms of the energy flux reduction for an average outdoor temperature of 10 °C (Fig. 7a), the time delay could be increased to up to 3 h by adjusting T_{pc}. It can be further increased by increasing the PCM volume fraction ϕ_c and/or the latent heat of fusion h_{sf}. Therefore, adding PCM to a building wall in an extremely hot or cold climate may still provide financial savings to the ratepayer if TOU pricing is available, by shifting the heating or cooling load to an off-peak time of day.

4.2.5. Effect of outdoor temperature

Fig. 8a plots the maximum energy flux reduction $E_{r,max}$ as a function of the average outdoor temperature $(T_{max} + T_{min})/2$ ranging from 5 to 35 °C for outdoor temperature amplitude $(T_{max} - T_{min})/2$ of 10 or 15 °C. The PCM volume fraction ϕ_c, latent heat of fusion h_{sf}, and phase change temperature window ΔT_{pc} were taken as 0.1, 180 kJ/kg, and 3 °C, respectively. Fig. 8a reveals that the maximum energy reduction could reach up to 40% and was achieved when the average outdoor temperature was about 22 °C for both outdoor temperature amplitudes of 10 and 15 °C. This was slightly higher than the imposed indoor temperature T_{in} of 20 °C. Furthermore, the maximum energy flux reduction $E_{r,max}$ decreased as the amplitude of the outdoor temperature oscillations increased. As the average outdoor temperature $(T_{max} + T_{min})/2$ approached extremely hot or cold conditions, the maximum

energy flux reduction $E_{r,max}$ reached a constant value of about 6%. This was equal to the energy flux reduction achieved for PCM volume fraction ϕ_c of 0.1 in absence of phase change. These results confirm that phase change had no effect on the daily energy flux reduction in extreme hot or cold climates. It may also explain why Chan [11] and Zwanzig et al. [12] observed small reductions in wall heat transfer in the hot climates of Hong Kong and Miami, FL, respectively. In fact, Chan [11] showed that the inner wall surface temperature remained above 28 °C for almost the entire cooling season. This was above the typical desired indoor temperature range and would therefore result in continuous cooling to accommodate a unidirectional heat flux. Additionally, the inner wall heat flux in Miami was unidirectional for nearly the entire summer week, as illustrated in Fig. 11 of Ref. [12]. However, the authors [11,12] attributed their findings to the choice of phase change temperature and not to the fact that the heat flux was unidirectional in the climates they considered.

Fig. 8b plots the optimum phase change temperature corresponding to the maximum energy flux reduction T_{pc,opt,E_r} as a function of average daily outdoor temperature ranging from 5 to 35 °C and for outdoor temperature amplitude of 10 and 15 °C. It shows that $E_{r,max}$ was achieved for an optimum phase change temperature T_{pc,opt,E_r} near the indoor temperature $T_{in} \pm 1$ °C, regardless of the average daily outdoor temperature. This may seem counterintuitive since one would a priori think that the PCM melting temperature should also depend on the outdoor temperature or the climate, as suggested in the literature [11,12,35].

Fig. 8c plots the maximum time delay $\tau_{d,max}$ as a function of the average outdoor temperature $(T_{max} + T_{min})/2$ ranging from 5 to 35 °C for outdoor temperature amplitude $(T_{max} - T_{min})/2$ of 10 or 15 °C. For the selected value of $\phi_c = 0.1$, the maximum time delay could reach up to about 3 h and was achieved when $(T_{max} + T_{min})/2$ and $(T_{max} - T_{min})/2$ were 10 °C. Additionally, $\tau_{d,max}$ decreased only slightly from 3 to 2 h as the average daily outdoor temperature increased from 5–10 to 35 °C. Fig. 8d plots the optimum phase change temperature corresponding to the maximum time delay T_{pc,opt,τ_d} as a function of average daily outdoor temperature and for outdoor temperature amplitude $(T_{max} - T_{min})/2$ of 10 or 15 °C. It shows that T_{pc,opt,τ_d} increased nearly linearly from 16 to 31 °C as $(T_{max} + T_{min})/2$ increased from 5 to 35 °C.

5. Conclusion

This study demonstrated that a composite wall containing microencapsulated PCMs can be accurately represented as a homogeneous wall with some effective thermal properties given by Eqs. (13)–(15). This time-dependent homogeneous thermal model was used to establish important design rules that can inform the selection of microencapsulated PCMs for concrete walls in various climates. First, adding microencapsulated PCM to concrete walls and increasing the latent heat of fusion both substantially reduced and delayed the thermal load on the building. Second, the phase change temperature leading to the maximum energy flux reduction was equal to the desired indoor temperature regardless of the climate conditions. Third, to achieve the maximum time delay, the optimum phase change temperature increased with increasing average outdoor temperature. Fourth, in extremely hot or cold climates, the use of PCM delayed the thermal load to take advantage of TOU pricing even though the energy flux reduction was not significant. Lastly, the phase change temperature window had little effect on the energy flux reduction and the time delay. This analysis can inform future simulations of composite walls containing microencapsulated PCMs in any climate.

Acknowledgement

This manuscript was prepared as a result of work sponsored by the California Energy Commission (Contract: PIR:-12-032), the U.S. National Science Foundation (CMMI: 1130028) and the University of California, Los Angeles (UCLA). It does not necessarily represent the views of the Energy Commission, its employees, the State of California, or the National Science Foundation. The Energy Commission, the State of California, its employees, contractors, and subcontractors make no warranty, express or implied, and assume no legal liability for the information in this document; nor does any party represent that the use of this information will not infringe upon privately owned rights. This manuscript has not been approved or disapproved by the California Energy Commission nor has the California Energy Commission passed upon the accuracy or adequacy of the information in this paper.

Appendix A. Supplementary material

Supplementary data associated with this article can be found, in the online version, at http://dx.doi.org/10.1016/j.enconman.2014.12.078.

References

[1] U.S. Energy Information Administration. Annual energy review 2011, Government Printing Office; 2012.
[2] U.S. Department of Energy. Buildings energy data book; 2011. <http://buildingsdatabook.eren.doe.gov>.
[3] Farid MM, Khudhair AM, Razack SAK, Al-Hallaj S. A review on phase change energy storage: materials and applications. Energy Convers Manage 2004;45(9):1597–615.
[4] Electricity markets: consumers could benefit from demand programs, but challenges remain, Tech. Rep. GAO-04-844, Government Accountability Office, Washington, DC, August 2004. <www.energy.ca.gov>.
[5] California Public Utilities Commission and Others. California long term energy efficiency strategic plan: achieving maximum energy savings in california for 2009 and beyond. San Francisco (CA): California Public Utilities Commission; 2008.
[6] Cabeza LF, Castellon C, Nogues M, Medrano M, Leppers R, Zubillaga O. Use of microencapsulated PCM in concrete walls for energy savings. Energy Build 2007;39(2):113–9.
[7] Jayalath A, Mendis P, Gammampila G, Aye L, Ngo T. Applications of phase change materials in concrete for sustainable built environment: a review. In: Proceedings of the international conference on structural engineering, construction, and management (ICSECM), Kandy, Sri Lanka, December 16–18, 2011, p. 1–13.
[8] Ling T-C, Poon C-S. Use of phase change materials for thermal energy storage in concrete: an overview. Constr Build Mater 2013;46:55–62.
[9] Zhu N, Ma Z, Wang S. Dynamic characteristics and energy performance of buildings using phase change materials: a review. Energy Convers Manage 2009;50(12):3169–81.
[10] Halford CK, Boehm RF. Modeling of phase change material peak load shifting. Energy Build 2007;39(3):298–305.
[11] Chan ALS. Energy and environmental performance of building façades integrated with phase change material in subtropical Hong Kong. Energy Build 2011;43(10):2947–55.
[12] Zwanzig SD, Lian Y, Brehob EG. Numerical simulation of phase change material composite wallboard in a multi-layered building envelope. Energy Convers Manage 2013;69:27–40.
[13] Khudhair AM, Farid MM. A review on energy conservation in building applications with thermal storage by latent heat using phase change materials. Energy Convers Manage 2004;45(2):263–75.
[14] Tyagi VV, Buddhi D. PCM thermal storage in buildings: a state of art. Renew Sustain Energy Rev 2007;11(6):1146–66.
[15] Pasupathy A, Velraj R. Effect of double layer phase change material in building roof for year round thermal management. Energy Build 2008;40(3):193–203.
[16] Sharma A, Tyagi VV, Chen CR, Buddhi D. Review on thermal energy storage with phase change materials and applications. Renew Sustain Energy Rev 2009;13(2):318–45.
[17] Baetens R, Jelle BP, Gustavsen A. Phase change materials for building applications: a state-of-the-art review. Energy Build 2010;42(9):1361–8.
[18] Kuznik F, David D, Johannes K, Roux J-J. A review on phase change materials integrated in building walls. Renew Sustain Energy Rev 2011;15(1):379–91.
[19] Tyagi VV, Kaushik SC, Tyagi SK, Akiyama T. Development of phase change materials based microencapsulated technology for buildings: a review. Renew Sustain Energy Rev 2011;15(2):1373–91.

[20] Zhou D, Zhao C-Y, Tian Y. Review on thermal energy storage with phase change materials (PCMs) in building applications. Appl Energy 2012;92:593–605.
[21] Salunkhe PB, Shembekar PS. A review on effect of phase change material encapsulation on the thermal performance of a system. Renew Sustain Energy Rev 2012;16(8):5603–16.
[22] Sarier N, Onder E. Organic phase change materials and their textile applications: an overview. Thermochim Acta 2012;540:7–60.
[23] Hunger M, Entrop AG, Mandilaras I, Brouwers HJH, Founti M. The behavior of self-compacting concrete containing micro-encapsulated phase change materials. Cem Concr Compos 2009;31(10):731–43.
[24] AL-Saadi SN, Zhai ZJ. Modeling phase change materials embedded in building enclosure: a review. Renew Sustain Energy Rev 2013;21:659–73.
[25] Voller V, Cross M. Accurate solutions of moving boundary problems using the enthalpy method. Int J Heat Mass Transfer 1981;24(3):545–56.
[26] Zhang D, Fung AS, Siddiqui O. Numerical studies of integrated concrete with a solid–solid phase change material. In: Proceedings of the 2nd canadian solar buildings conference, Calgary, Canada, June 10–14, 2007.
[27] Lamberg P, Lehtiniemi R, Henell A-M. Numerical and experimental investigation of melting and freezing processes in phase change material storage. Int J Therm Sci 2004;43(3):277–87.
[28] Darkwa J, Su O. Thermal simulation of composite high conductivity laminated microencapsulated phase change material (MEPCM) board. Appl Energy 2012;95:246–52.
[29] Gowreesunker BL, Tassou SA, Kolokotroni M. Improved simulation of phase change processes in applications where conduction is the dominant heat transfer mode. Energy Build 2012;47:353–9.
[30] Ogoh W, Groulx D. Stefan's problem: validation of a one-dimensional solid-liquid phase change heat transfer process. In: Proceedings of the COMSOL conference, Boston, MA, October 7–9, 2010.
[31] Heim D. Isothermal storage of solar energy in building construction. Renew Energy 2010;35(4):788–96.
[32] Castellón C, Günther E, Mehling H, Hiebler S, Cabeza LF. Determination of the enthalpy of PCM as a function of temperature using a heat-flux DSC: a study of different measurement procedures and their accuracy. Int J Energy Res 2008;32(13):1258–65.
[33] Zhou G, Zhang Y, Wang X, Lin K, Xiao W. An assessment of mixed type PCM-gypsum and shape-stabilized PCM plates in a building for passive solar heating. Sol Energy 2007;81(11):1351–60.
[34] Zhou G, Zhang Y, Lin K, Xiao W. Thermal analysis of a direct-gain room with shape-stabilized PCM plates. Renew Energy 2008;33(6):1228–36.
[35] Diaconu BM, Cruceru M. Novel concept of composite phase change material wall system for year-round thermal energy savings. Energy Build 2010;42(10):1759–72.
[36] Mathieu-Potvin F, Gosselin L. Thermal shielding of multilayer walls with phase change materials under different transient boundary conditions. Int J Therm Sci 2009;48(9):1707–17.
[37] Hembade L, Neithalath N, Rajan SD. Understanding the energy implications of phase-change materials in concrete walls through finite-element analysis. J Energy Eng 2013;140(1):04013009.
[38] Mackey CO, Wright LT. Periodic heat flow-homogeneous walls or roofs. ASHVE Trans 1944;50:293–312.
[39] Kissock K, Limas S. Diurnal load reduction through phase-change building components. ASHRAE Trans 2006:509–17.
[40] Thiele AM, Kumar A, Sant G, Pilon L. Effective thermal conductivity of three-component composites containing spherical capsules. Int J Heat Mass Transfer 2014;73:177–85.
[41] PureTemp 20 Technical Information, Tech. Rep., Entropy Solutions Inc., Minneapolis, MN; 2011.
[42] Typical engineering properties of high density polyethylene, Tech. Rep., INEOS Olefins & Polymers USA, League City, TX; 2009.
[43] Incropera FP, Bergman TL, Lavine AS, DeWitt DP. Fundamentals of heat and mass transfer. New York City (NY): John Wiley & Sons; 2011.
[44] Bridgman PW. A complete collection of thermodynamic formulas. Phys Rev 1914;3(4):273–81.
[45] Felske JD. Effective thermal conductivity of composite spheres in a continuous medium with contact resistance. Int J Heat Mass Transfer 2004;47:3453–61.
[46] Hashin Z. Assessment of the self consistent scheme approximation: conductivity of particulate composites. J Compos Mater 1968;2(3):284–300.
[47] UCLA Energy Design Tools Group. Climate Consultant; 2014. <http://www.energy-design-tools.aud.ucla.edu>.
[48] Awbi HB, Hatton A. Mixed convection from heated room surfaces. Energy Build 2000;32(2):153–66.
[49] Alawadhi EM. Thermal analysis of a building brick containing phase change material. Energy Build 2008;40(3):351–7.
[50] International Organization for Standardization. ISO standard 6946: building components and building elements: thermal resistance and thermal transmittance - calculation method; 2007.
[51] Darkwa K, O'Callaghan PW, Tetlow D. Phase-change drywalls in a passive-solar building. Appl Energy 2006;83(5):425–35.
[52] Alexiades V. Mathematical modeling of melting and freezing processes. Boca Raton (FL): CRC Press; 1992.